Available online at www.sciencedirect.com

ScienceDirect

Procedia Computer Science 181 (2021) 511–518

Procedia Computer Science

www.elsevier.com/locate/procedia

CENTERIS - International Conference on ENTERprise Information Systems / ProjMAN - International Conference on Project MANagement / HCist - International Conference on Health and Social Care Information Systems and Technologies 2020

Methods to avoid being affected by non-zero closure phase in InSAR time series analysis in a multi-reference stack

Urs Wegmüller*, Christophe Magnard, Charles Werner, Tazio Strozzi, Rafael Caduff, Andrea Manconi

Gamma Remote Sensing AG, Worbstrasse 225, CH-3073 Gümligen, Switzerland

Abstract

This work discusses InSAR time series analysis using *multi-reference stacks* with exclusively short time intervals. A 5 months long stack of Sentinel-1 acquisitions over a high alpine territory that includes fast moving landslides is used. Use of the *multi-look phases* becomes problematic due to non-zero closure phase. The errors induced by non-zero phase closure can be avoided by the use of *single-look phases* for all scatterers, including distributed scatterers. A weighted least-squares solution of the deformation time-series is obtained using the *multi-reference stack* interferometric single-*look phases*. Quality control is done during the regression analysis, the conversion to the time series, and considering the temporal coherence. Spatial filtering of the *single-look phase* time series can be used to further reduce the phase noise present in areas with intermediate coherence levels.

© 2021 The Authors. Published by Elsevier B.V.
This is an open access article under the CC BY-NC-ND license (https://creativecommons.org/licenses/by-nc-nd/4.0)
Peer-review under responsibility of the scientific committee of the CENTERIS - International Conference on ENTERprise Information Systems / ProjMAN - International Conference on Project MANagement / HCist - International Conference on Health and Social Care Information Systems and Technologies 2020

Keywords: DInSAR; PSI; SBAS; time-series analysis; multi-reference stack; distributed scatterers; multi-look phases; single-look phases; fast non-uniform motion; displacement monitoring;

1. Introduction

1.1. Objectives of using distributed scatterers and a multi-reference stack based procedure

Interferometric Synthetic Aperture Radar (InSAR) based methods are playing an increasingly important role in different phases of the management of gravitational natural hazards, e.g. in Switzerland [1]. Thanks to terrestrial

* Corresponding author. Tel.: +41-31-9517005 ; fax: +41-31-9517008 .
E-mail address: wegmuller@gamma-rs.ch

1877-0509 © 2021 The Authors. Published by Elsevier B.V.
This is an open access article under the CC BY-NC-ND license (https://creativecommons.org/licenses/by-nc-nd/4.0)
Peer-review under responsibility of the scientific committee of the CENTERIS - International Conference on ENTERprise Information Systems / ProjMAN - International Conference on Project MANagement / HCist - International Conference on Health and Social Care Information Systems and Technologies 2020
10.1016/j.procs.2021.01.197

radars ([2]) and satellite SAR becoming more abundantly available, e.g. through the Sentinel-1 constellation [3] with acquisitions over most of Europe every 6 days in both ascending and descending orbits, InSAR can also provide a relevant contribution to the monitoring of fast and potentially accelerating landslides [4,5]. Multi-temporal repeat-pass satellite SAR data stacks are regularly used to map and monitor ground surface deformation. The applied processing methodologies can be adapted to obtain optimized results for a given case, depending on target and SAR data characteristics. In the specific application case discussed here, we retrieve a deformation time series over a high alpine area in the Swiss Alps.

The investigated area includes the known rapidly moving Moosfluh landslide. During the past 30 years the motion rate has increased from about 4cm/year during the 1990's to more than 20cm/year in 2008 [4,6]. In the late summer 2016, a sudden acceleration was reported, with surface velocity rates reaching maximum values of about 80cm/day [7]. During the following winter (November 2016–March 2017) the ground deformation decelerated, however, rates were still high compared with previous winter periods. In 2017 the fastest deformation rates, up to 25cm/day, were reached at the beginning of September. After that the rates declined during the winter and increased again in the summer 2018 to reach deformation rates around 20cm/day in Sep. 2018 [7].

Using Sentinel-1 data acquired during the snow-free period of 2019 our objective is to monitor the rates for this period. Based on the experience from the past the movement was most likely expected to be non-uniform in time. A significant fraction of the area investigated is above the forest line, and of course most of the area is non-urban. For our investigation we selected 25 Sentinel-1 scenes of summer and fall 2019, mostly with a 6-day repeat intervals. Considering the presence of deformation rates > 10cm/year and non-uniform movements we decided to use a *multi-reference stack* including all the pairs with short temporal intervals of 6, 12, and 18 days. Besides getting a reliable result for the fastest moving landslides in the area, an important objective was to get deformation information on more slowly moving and stable areas (rates < 5cm/year) with a reasonable accuracy (e.g. < 2cm/year). To achieve a good spatial coverage in this area we decided to include both *point-like scatterers* and *distributed scatterers* in our analysis. Including only data of one snow free season we expect to achieve a good spatial coverage.

1.2. Terminology

In our reporting we try to carefully define the characteristic of what we do, avoiding using names of methods frequently used in the community such as SBAS or PSI, that have, unfortunately, become quite meaningless in that they are used for a wide range of methods. In the following we clarify a few important terms we will be using.

A *single-reference stack* is a stack of pairs with one common reference scene. A *multi-reference stack* is a stack of pairs with more than one reference scene. In our analysis we use a *multi-reference stack* including for each acquisition the pairs with the following 3 scenes acquired. In this way, each time interval is covered by multiple redundant observations.

Concerning the scattering mechanisms we distinguish *point-like scatterers* and *distributed scatterers*. Examples for *point-like scatterers* are corner reflectors and spheres. But *point-like scatterers* are also often found in urban settings and are more generally related to infrastructure. The relevant characteristic of a *point-like scatterer* is that the phase of the scattered signal is isotropic over an angular range larger than the angular range defined by the critical baseline. A scatterer is a *point-like scatterer* if the dimension of the dominant scattering element is significantly smaller than the dimension of the pixel. A *distributed scatterer* has a large number of scattering elements distributed over the pixel area. Bare and vegetated soils are typical *distributed scatterers*. For *distributed scatterers* the typical radar speckle phenomena are observed. The phase of the scattered signal varies with the scattering angle and becomes decorrelated at the angle corresponding to the critical baseline. For data stacks that include long spatial baselines (e.g. ERS, ENVISAT) using *point-like scatterers* has the advantage that the phase can be interpreted even for pairs with baselines greater than the critical baseline. For data stacks that include exclusively short spatial baselines (e.g. Sentinel-1) the difference between *point-like scatterers* and *distributed scatterers* become less evident. Nevertheless, it is still possible to identify *point-like scatterers* e.g. using the spectral diversity criteria [8,9].

In an interferometric analysis *single-look* and *multi-look* interferometric *phases* can be used. In the case of data stacks with very long spatial baselines identifying *single-look* scatterer elements potentially suited for a time-series analysis based on a low amplitude variability means that *point-like scatterers* are selected. Applying the same

criterium to a stack with only short spatial baselines means that *point-like* and *distributed scatterers* that remain coherent over the time are selected. Hence using *point-like scatterers* and using *single-look phases* is not the same! Similarly, *multi-look phases* can be used for both *point-like scatterers* and *distributed scatterers*. The main idea behind using *multi-look phases* is to reduce the phase noise in areas with lower coherence.

1.3. Contents

In the following we will first present an initial processing done using a combination of *single-look* and *multi-look phases*. Comparing the characteristics for the two elements reveals a problematic characteristic of the *multi-look phases* when used with a *multi-reference stack* of exclusively short time intervals, namely problems related to the presence of non-zero closure phase. The problems are discussed and then possible solutions to avoid the problems are presented and assessed. Finally, conclusions are drawn and recommendations given.

2. Multi-reference stack analysis over Aletsch area

Considering our objectives, we conducted an initial time series analysis. We used 25 Sentinel-1 acquisitions acquired between 4-Jun-2019 and 1-Nov-2019. Except for one date (14-Sep) acquisitions were taken every 6 days. Based on the 25 scenes we defined a *multi-reference stack* with 66 pairs with 6, 12, and 18 days intervals. All spatial baselines are short, with a longest perpendicular baseline of 163m and 63 perpendicular baselines shorter than 100m.

The SLCs are co-registered considering the double-difference phase in the burst overlap areas and a range oversampling with a factor two is applied.

In our processing we included *single-look phases* as well as *multi-look phases*. The candidate pixels for the *single-look phases* are to about 60% identified using the spectral diversity criteria of the GAMMA IPTA Software [8,9] and to about 40% using the low temporal amplitude variation criterium. Accordingly, the *single-look phases* used correspond primarily to *point-like scatterers*. The *multi-look phases* are determined using 27 range looks and 3 azimuth looks of the range oversampled SLC. Except for layover, shadow and very low average coherence (mainly the glaciers which decorrelate because of their fast motion and melting) *multi-look phases* are selected for the entire area. For the selected SLC area of 8100 range pixels x 1500 azimuth lines this resulted in about 300 x 500 *multi-look phases* minus a few percent of rejected as layover, shadow or having very low average coherence < 0.1. The differential interferogram phases for the *single-look* elements (75610) and the *multi-look* elements (107955) were combined into one list with 183565 elements in vector data format.

In the actual InSAR time series analysis we distinguish as the two main steps, the derivation of reliably unwrapped phases for the differential interferogram pairs of the *multi-reference stack* and the interpretation of the phases with respect to parameters as the topographic height correction, line-of-sight displacement, and atmospheric path delay. In both steps quality parameters are determined and used to limit the solution to elements for which the solution meets a minimum quality requirement.

In the phase unwrapping step, the regression analysis on the spatio-temporal phase differences is an important tool. A significant feature of this analysis is to use a one-dimensional regression of the phase with respect to the perpendicular baseline, to solve only for the scatterer height corrections. This contrasts with a two-dimensional analysis that includes the interferogram time intervals to solve for both height correction and linear deformation rate. The short time-intervals of the multi-reference stack permit this simplification. that improves the robustness of the solution. For a line-of-sight (LOS) deformation rate of 10cm/year the deformation phase over 18 days is only 1.1 radian which should still not cause significant unwrapping errors. Initially, the regressions are calculated for pairs of elements with relatively short spatial separation on the ground, so that the related atmospheric phases remain small. Once atmospheric phase screens have been estimated and subtracted the regressions are calculated relative to the spatial reference location, a village not far from the main landslide of interest at a similar topographic height as the landslide. The unwrapping is initially done as part of the regression analysis, but the result is spatially checked and if necessary corrected. The point height corrections determined are not very accurate because of the short spatial baselines of the pairs. The determined corrections clearly show a low-frequency component that most likely relates to atmospheric phase delays present on certain dates. Assuming that the used height reference is correct at km scale, we only correct the heights with the high frequency component of the determined correction. The atmospheric path

delays determined and corrected for include a hydrostatic and a non-hydrostatic component. For the hydrostatic component a linear relation with the topographic height is used as model. The remaining part is the non-hydrostatic component and is assumed to be spatially smooth. The atmospheric phase components can be spatially interpolated to elements without high quality regression. Applying the determined height corrections and atmospheric path delay phases improves the quality of the regressions which permits to include further elements and to consolidate the unwrapping solution. The phase standard deviation threshold used in the later regressions was 1.2 radian and resulted in unwrapped phases for 159'000 elements.

Except for the orbital and topographic phase, the unwrapped phase components are then summed up to obtain the total unwrapped differential interferometric phase for each layer of the *multi-reference stack*. This phase includes deformation phase, atmospheric phase as well as phase noise. A singular value decomposition (SVD) least-squares solution is used to combine this unwrapped, partially redundant, short-interval *multi-reference stack* phases into phase time series relative to the first acquisition. Initially no temporal smoothing is applied, so the objective is not to derive a time series that corresponds to the deformation phase only, but a time series that corresponds to the deformation phase plus the atmospheric phase plus the phase noise. For *single-look phases* the SLC of a specific acquisition has one specific value and so it is expected that the time series found should nicely follow the individual phase values. The determined unwrapped *multi-reference stack* phases should almost perfectly match with the related temporal phase differences in the time series – as is confirmed by phase standard deviations from the time series < 0.1 radian. The histogram of the phase standard deviations shows for the *single-look* elements a clear maximum for the class 0.0 to 0.1 radian, then almost no values at all in the next intervals up to 0.5 radian and then some values in the intervals with standard deviations > 0.5 radian (Figure 1). For the elements in the 0.0 to 0.1 radian class our interpretation is that the phase unwrapping is perfectly consistent between all the partially redundant differential interferometric phases of the *multi-reference stack*. Even a single ambiguity error in the unwrapping will cause a phase standard deviation > 0.5 radian. Consequently, this phase standard deviation determined in the SVD can be used to qualify the consistency of the phase unwrapping, and in the case of few individual inconsistencies the phase differences from the time series can be used as a model to correct some unwrapping errors. For the *multi-look phase* elements, the standard deviation of the phase values behaves differently. There are fewer values in the 0.0 to 0.1 radian class but then also a significant number of values in all the following classes (Figure 1).

Using assumptions on the spatial and temporal characteristics of the phase time series was then split into deformation phase (temporally smooth), hydrostatic (linear dependence on topographic height), non-hydrostatic atmospheric phase (spatially smooth) and phase noise (temporally and spatially uncorrelated). Concerning non-uniform motion, we assume that non-uniform motion is either present at very local scale (< 500m) or in areas with a very high average deformation rate. Non-uniform motion at a spatial scale > 500m that is not in an area with a high average deformation rate (> 10cm/year) is not identified but ends up in the atmospheric path delay phase. On the other hand, this assumption avoids getting more or less non-uniform deformation at cm level related to atmospheric path delay variation. Based on the deformation time series from the described methodology, average deformation rates are determined and visualized separately for *single-look* (Fig. 5a) and *multi-look phases* (Fig. 5b).

3. Problem caused by non-zero closure phase of multi-look phases

Using *multi-look phases* a better spatial coverage could be achieved, even more so if the *multi-look phases* are used in addition to the *single-look phases*. Nevertheless, two relevant problems were encountered in using the *multi-look phases*. The first one was encountered in the phase unwrapping consistency checking done along the connection of the *multi-reference stack* DInSAR phases into a single time series. For *single-look phases* very low phase standard deviations are a reliable confirmation that the DInSAR phases were consistently unwrapped. As shown in Fig. 1 all levels of phase standard deviations occur for the *multi-look phases* and therefore it is not clear if a phase standard deviation of 0.5 radian relates to an unwrapping inconsistency. The reason is the non-zero closure phase [10-11] in the multi-look case. Figs. 2 to 4 show for a triplet A-B, B-C, and A-C the differential interferogram with the longest time interval, and the unfiltered and spatially filtered closure phase (defined as: $\text{phase}_{A\text{-}B} + \text{phase}_{B\text{-}C} - \text{phase}_{A\text{-}C}$). For the *multi-look phases* used in our processing (27 range oversampled looks x 3 azimuth looks) the closure phase shows a noise-like spatial variation at a level up to about 1.0 radian. Additional spatial filtering reduces the level of the closure phase but not necessarily to zero as discussed in the literature [10-13].

The second problem also relates to the non-zero closure phase. In the case of *single-look phases* the reconstructed time series is perfectly guided through the values of the acquisitions. In the multi-look case, the time series A-B-C will not perfectly match with A-C because of the different answer provided by A-B + B-C. This means an error is introduced and this error propagates along the time series. Assuming the non-zero closure phase is a random term the error propagation would be similar to a random walk, so over more steps the error would, on average, become larger proportional to the square root of the number of steps. If the error term is systematic, the error could even increase linearly with the number of steps. It could be systematic, for example, if it relates to the growth of the sparse vegetation on the ground. Probably the error is a combination of a more random and a more physically based term. Based on Fig. 3, we assume the error for the individual step is of the order of 0.5 to 1.0 radian. Hence for the five months duration time series with 25 acquisitions, the propagated error can become 3 to 6 radians, corresponding to LOS deformation errors of 1.4cm to 2.8cm, or 3.3cm/year to 6.6cm/year expressed as deformation rate errors.

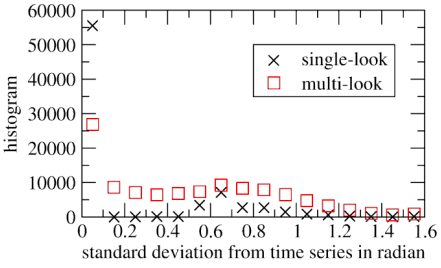


Fig. 1. Histogram of phase standard deviations obtained in the transformation of the unwrapped *multi-reference stack* phases to phase time series for *single-look* and *multi-look* elements.

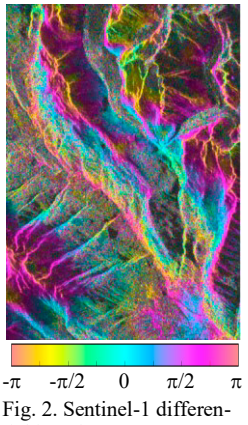


Fig. 2. Sentinel-1 differential interferogram 2. Oct. 2019 to 14. Oct. 2019

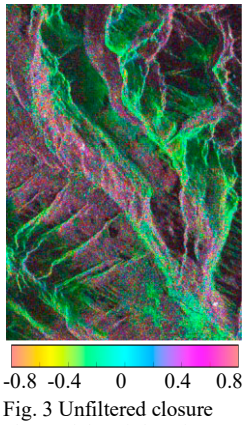


Fig. 3 Unfiltered closure phase of the triplet of 2., 8., and 14. Oct. 2019.

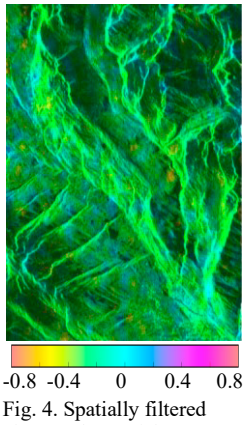


Fig. 4. Spatially filtered closure phase of the same triplet as in Fig. 3.

4. Introduction and assessment of possible solutions

4.1. Thresholding on closure phase level

As discussed, the level of the closure phase relates strongly to the phase standard deviation estimated in theLeast-Squares solution step implemented with SVD. Applying a low threshold to the estimated phase standard deviation restricts the result to elements with a lower closure phase error and therefore lower overall errors in the deformation history and rate estimation. In fact, this is what was done in getting the result shown in Fig. 5b.

4.2. Spatial filtering of the multi-look multi-reference stack phases

Applying a spatial filtering on the multi-look *multi-reference stack* phases permits reducing the closure phase error (Fig. 4) and therefore the resulting deformation estimation errors. Nevertheless, spatial filtering reduces the resolution. Furthermore, the effect of areas with very low coherence on the result is not so clear. A possible way to avoid being too much influenced by elements with too low coherence is to mask such areas before the filtering.

4.3. Including long-interval pairs into the multi-reference stack

Including pairs with a long temporal interval is a way minimize biased time series estimates. Nevertheless, the advantages of only including short interval pairs, namely achieving good spatial coverage and including fast and non-uniform motion into the result are lost. Furthermore, including more pairs is computationally less efficient, especially if all pairs (in the case of the 25 scenes this means 276 pairs) are included.

4.4. Considering a single- reference stack

Using a *single-reference stack* avoids being affected by non-zero closure phase. Nevertheless, the advantages of using a *multi-reference stack* with short interval pairs only, namely achieving a good spatial coverage and including fast and non-uniform motion into the result are lost.

4.5. Considering only single-look phases

In the processing described in Section 3, *single-look phases* were used for identified *point-like scatterer* candidates, whereas *multi-look phases* were considered for all areas, excluding layover, shadow and very low average coherence (< 0.1). Alternatively, we propose here to use *single-look phases* everywhere. In order to do this systematically, we selected all range oversampled SLC pixels except those in layover, shadow and very low coherence areas (→ 8723067 elements instead of 183565 considered in the initial processing). Having available the solution for the initial candidates the atmospheric path delay phases for the *multi-reference stack* pairs could be derived by spatial filtering and interpolation. As for the initial list height corrections, the unwrapped phases were then determined using one-dimensional regression analysis on the *multi-reference stack*. Using a threshold on the standard deviation of the linear fit of 1.2 radians, yielded 1439907 points accepted in the solution. In the calculation of the time series from the *multi-reference stack* phases using the SVD solver, 833485 elements were accepted as consistently unwrapped, and out of these 806317 have a temporal coherence larger than 0.5. The related result is shown in Fig. 5c.

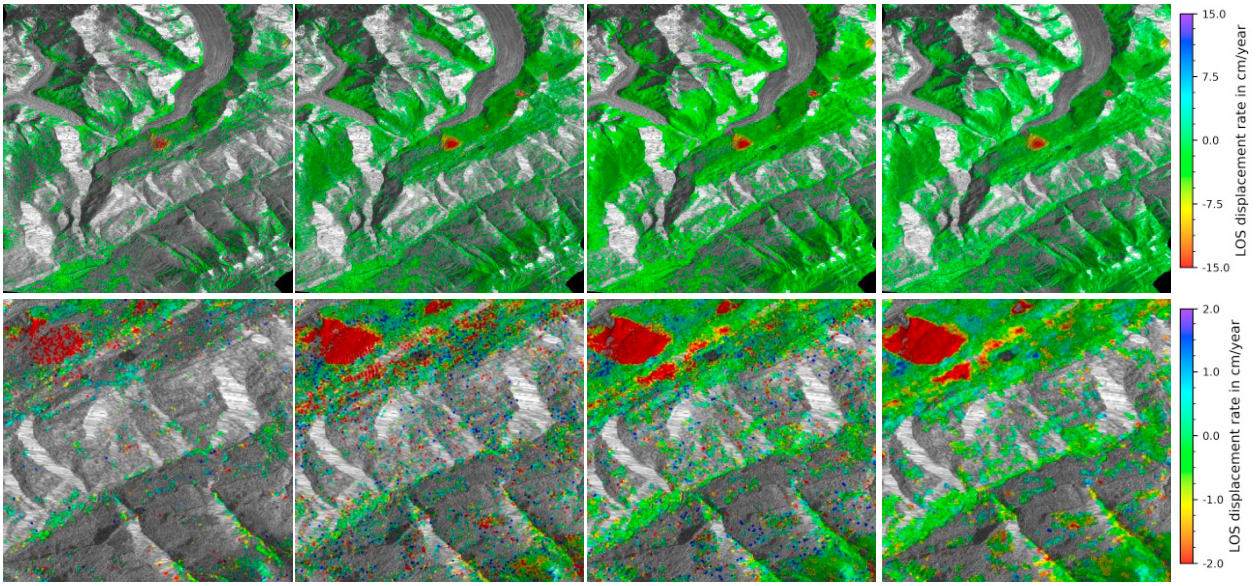
4.6. Considering only single-look phases and applying spatial filtering after combination into time-series

Applying spatial filtering and interpolation to the result described in 4.5 and using this as a model to unwrap all the DInSAR *single-look phases* of the *multi-reference stack* and checking these in the SVD step for consistency, the number of consistently unwrapped phases could be increased to 2088986 elements. For the resulting time series, we estimated the temporal coherence, removed all elements with coherence values below 0.5 and applied spatial filtering on the remaining 1519875 elements with a filter radius of 50 meters. The spatially filtered solution was only accepted if the filtering included at least 9 elements. For these spatially filtered phase time series we determined again a temporal coherence like parameter (values are higher because of the filtering applied) and rejected values with temporal coherence values below 0.9, which resulted in an accepted filtered solution for 1449809 elements. The related result is shown in Fig. 5d.

4.7. Discussion of results

In the initial analysis both *single-look phases* corresponding to *point-like scatterers* and *multi-look phases* were considered. The part of the result corresponding to the *multi-look phases* provides a more complete spatial coverage but the result appears noisier (Fig. 5b) than the result based on the *single-look phases* from *point-like scatterers* (Fig. 5a). For this stack that covers a total of only 5 months, using *single-look phases* alone avoids the problem with the non-zero closure phase encountered for *multi-look phases* and provides a solution for a much larger number of elements with a clearly better spatial coverage (Fig. 5c). More restrictive quality checks, checking of the spatial consistency of the result and spatial filtering of the time series can be used to substantially reduce the noise in the result (Fig. 5d) without significant loss of spatial coverage.

Notice that all results clearly show the deformation of the Moosfluh landslide. While the displacement rates reached in Sep. 2017 and Sep. 2018 maximum values of the order of 20cm/day the LOS displacement rates observed for 2019 remained below 20cm/year, with highest rates in mid-summer and a deceleration in fall (Fig. 6,7). To exclude a possible massive underestimation of the motion rate in the time-series analysis we also considered short-interval differential interferograms. Observing less than half a phase cycle, respectively 1.4cm of LOS displacement for 18 days confirmed the estimated maximum rates.



a) *Single-look phase* elements of initial solution.

b) *Multi-look phase* elements of initial solution.

c) Solution using all *single-look phase* elements without spatial filtering of phase time series.

d) Solution using all *single-look phase* elements with spatial filtering of phase time series.

Fig. 5. Linear deformation rate results for different processing approaches shown in the top row for a larger section using a color scale between -15cm/year and +15cm/year and in the bottom row for a smaller section using a color scale between -2cm/year and +2cm/year.

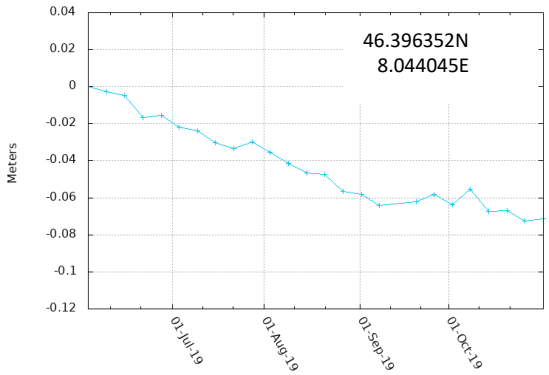


Fig. 6 LOS deformation time series for a location in the faster part of the Moosfluh landslide extracted from the result shown in Fig. 5c (spatially unfiltered).

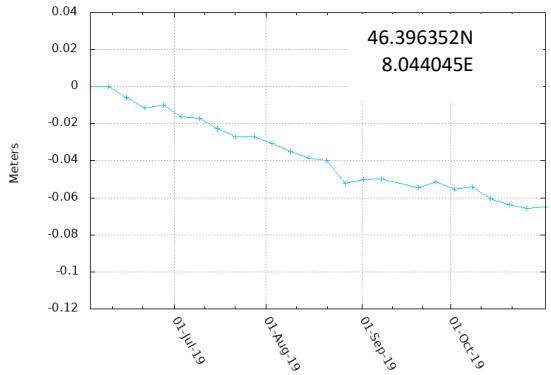


Fig. 7 LOS deformation time series for same location as in Fig. 6 extracted from the result shown in Fig. 5d (spatially filtered).

5. Conclusions and recommendations

The phase time series of *single-look phases* perfectly follows the phases of the individual acquisitions, if the unwrapping of all pairs is fully consistent. Accordingly, the phase standard deviation of the unwrapped phases of the pairs of the *multi-reference stack* from the time series from the SVD solver is very close to zero. An increased phase standard deviation (e.g. 0.7 radian) reliably indicates the presence of at least one unwrapping inconsistency. For *multi-look phases* the situation is different because of non-zero closure phases. For *multi-look phases* with about 40 looks and triplets with 6, 6, and 12 days intervals we observed non-zero closure phase levels of the order of 1 radian. As a consequence, the phase standard deviation of the unwrapped phases of the pairs of the *multi-reference stack* from the time series result is no longer very close to zero and so it is no longer possible to reliably check if the phase unwrapping is fully consistent. Furthermore, using the unwrapped multi-look phases to solve for the time series results in significant noise and biases.

Using a *single-reference stack* avoids the problem with the non-zero closure phases but relies on long-term coherent scatterers and has limitations in retrieving very fast and non-uniform movements. Using a *multi-reference stack* that also includes long-term interferograms, e.g. selecting all possible pairs, strongly reduces the problem with the non-zero closure phases but is computationally more demanding and relies on long-term coherent scatterers. One of the main ideas of using *multi-look phases* is to better include areas with *distributed scatterers*. Knowing that *single-look* elements can also be *distributed scatterers* we decided to use exclusively *single-look phases* to avoid the problem with the non-zero closure phases. Using all the *single-look phases* was found in this work to be an adequate approach for the *multi-reference stack* analysis. Less suited elements are rejected based on low quality in the *multi-reference stack* regression or later on in the unwrapping consistency checking done in the SVD step. Furthermore, the temporal coherence is used as a quality measure to accept or reject the solution for each location. Optionally, the *single-look phases* based time series can be spatially filtered to reduce noise or outliers can be rejected considering the spatial consistency of the result. In doing this a thresholding on the available points in the filter was used to avoid having less filtered more noisy isolated elements in the solution. The approach using all *single-look phases* provided the best spatial coverage and fully includes the result derived for the *single-look* scatterers that correspond to *point-like scatterers* but also includes many additional *distributed scatterers*.

As demonstrated *multi-reference stacks* of short time interval Sentinel-1 pairs over areas with *distributed scatterers* can be successfully used to map fast and non-uniform displacements. This finding is relevant for the application of InSAR time series methods to the mapping and monitoring of displacement rates > 10cm/year and non-uniform high alpine landslides and rock instabilities.

6. Acknowledgments

This work was supported by the EUROSTARS Project E!113220 RAMON (EUREKA, co-financed by Innosuisse). ESA/Copernicus are acknowledged for the Sentinel-1 data used.

7. References

[1] Wegmüller, U.; Caduff, R.; and T. Strozzi: Einsatz von Radarmethoden im Geomonitoring der Schweiz. In: Tagungsband Geomonitoring 2020, S. 3-15. DOI: https://doi.org/10.15488/9336

[2] Caduff, R., Schlunegger, F., Kos, A., & Wiesmann, A. (2014). A review of terrestrial radar interferometry for measuring surface change in the geosciences, Earth Surf. Processes Landforms, 02/2015; 40(2). DOI:10.1002/esp.365.

[3] ESA Webpage for Sentinel-1, 2020; https://sentinel.esa.int/web/sentinel/missions/sentinel-1

[4] Kos A., F. Amann, T. Strozzi, R. Delaloye, J. von Ruette and S. Springman, Contemporary glacier retreat triggers a rapid landslide response, Great Aletsch Glacier, Switzerland, Geophys. Res. Lett., 43, doi:10.1002/2016GL071708, 2016.

[5] Caduff R. and T. Strozzi, Terrestrial radar interferometry monitoring during a landslide emergency 2016, Ghirone, Switzerland. In: Mikoš M, Arbanas Ž, Yin Y, Sassa K (eds) Advancing culture of living with landslides, vol 3. p 301-309. Springer Int. Publ., Switzerland, 2017.

[6] Strozzi, T.; Delaloye, R.; Kääb, A.; Ambrosi, C.; Perruchoud, E.; and U. Wegmüller, Combined observations of rock mass movements using satellite SAR interferometry, differential GPS, airborne digital photogrammetry, and airborne photography interpretation. J. Geophys. Res. 2010, 115.

[7] Manconi A., P. Kourkouli, R. Caduff, T. Strozzi, and S. Loew. Monitoring Surface Deformation over a Failing Rock Slope with the ESA Sentinels: Insights from Moosfluh Instability, Swiss Alps. Remote Sensing, 10(5), 2018.

[8] Wegmüller U., C. Werner, T. Strozzi, and A. Wiesmann, „Multi-temporal interferometric point target analysis", in Analysis of Multi-temporal remote sensing images, Smits and Bruzzone (ed.), Series in Remote Sensing, Vol. 3, World Scientific (ISBN 981-238-915-61), pp. 136-144, 2004.

[9] Gamma Software Information, 2020; https://www.gamma-rs.ch/uploads/media/GAMMA_Software_information.pdf.

[10] De Zan F., M. Zonno, and P. Lopez-Dekker, "Phase Inconsistencies and Multiple Scattering in SAR Interferometry," IEEE Trans. Geoscience and Remote Sensing, vol. 53, no. 12, pp. 6608–6616, Dec. 2015.

[11] Zwieback S., X. Liu, S. Antonova, B. Heim, A. Bartsch, J. Boike, and I. Hajnsek, "A Statistical Test of Phase Closure to Detect Influences on DInSAR Deformation Estimates Besides Displacements and Decorrelation Noise: Two Case Studies in High-Latitude Regions," IEEE Trans. Geoscience and Remote Sensing, vol. 54, no. 9, pp. 5588–5601, Sep. 2016.

[12] De Zan F., A. Parizzi, P. Prats-Iraola, and P. Lopez-Dekker, "A SAR interferometric model for soil moisture," IEEE Trans. Geoscience and Remote Sensing, vol. 52, no. 1, pp. 418–425, 2013.

[13] De Zan F. and G. Gomba, "Vegetation and soil moisture inversion from SAR closure phases: First experiments and results," Remote sensing of environment, vol. 217, pp. 562–572, 2018.